



Preliminary comparative study on the behaviour of highly-loaded glue laminated timber and wood-CFRP composite beams exposed to local fire

B. Kawecki¹ · M. Pieńko¹ · T. Lipecki¹ · A. Stachowicz²

Received: 21 February 2022 / Accepted: 17 August 2023 / Published online: 27 August 2023
© The Author(s) 2023

Abstract

The paper presents a complex solution for testing loaded structural-sized glue laminated timber and innovative wood-carbon fibre reinforced polymers (CFRP) composite beams exposed to local fire. It shows the entire procedure from predicting a static behaviour and a combustion time (from reaching 300 °C temperature of the element up to its fracture) of the tested elements, designing and building an experimental stand, through conducting preliminary tests and discussing the results. The research included combustion of three glue laminated timber (BSH) and three wood-CFRP composite (BSH-CFRP) structural-sized beams in the most loaded section (region of highest bending moment) under three-point bending. A furnace was set under the centre of the beam on one-third of its span. The dimensions of the basket are based on physical properties of firewood providing proper burning conditions of the elements. The self-designed and self-constructed experimental stand enabled applying high load and provided a stable loading during local fire exposure. The preliminary tests showed that using CFRP tapes inside the section may both increase or decrease fire resistance of wooden members depending on the width of wood material covering CFRP tape. CFRP tapes provide a different nature of beam failure, which is changing from sudden fracture (BSH) to plastic flow of the material (BSH-CFRP).

1 Introduction

Nowadays, composites are used in various industry branches. Combining materials with unique properties allows to optimise the load-bearing elements and to adapt their strength to the expected loads. Many material compositions are described in the literature. One of the not fully investigated is the composite made of wood and carbon fibre reinforced polymers (CFRP).

Strengthening existing structural members by gluing CFRP to their outer surface enables to increase the stiffness and strength of the construction. However, only single studies on such systems, under extreme conditions, such as elevated temperatures, are available—mainly in concrete structures. The glass transition temperature of the epoxy matrix, in which the carbon fibres are embedded, is between 60 and

120 °C. Heating the CFRP composite to such a temperature causes its decomposition. This can endanger the safety of the entire reinforced structure. Hence, to limit the possibility of exposure to high temperatures, thick layers of insulating sheathing materials are used. This results in a significant increase in the cost of the entire technology.

Suitable solution can be to glue the CFRP tape inside the wooden cross-section at the stage of production of structural elements. Wood is an insulator with a unique property, such as charring at high temperature (ca. 300 °C). The charred layer protects the inside of the section, where the temperature remains constant at room temperature (20–40 °C). Thus, the proper location of the CFRP tape may allow for its reliable work for the required time.

1.1 Static tests on wood-CFRP composites

The current literature is rich in static studies of composites composed of wood and CFRP, done by various research centres around the world. Both strengthening the existing structures and testing newly manufactured elements has been carried out. A general review of reinforcing techniques for wooden girders has been presented, for example, by Schober

✉ B. Kawecki
b.kawecki@pollub.pl

¹ Lublin University of Technology, Faculty of Civil Engineering and Architecture, Lublin, Poland

² ABIES Poland Ltd., Pszów, Poland

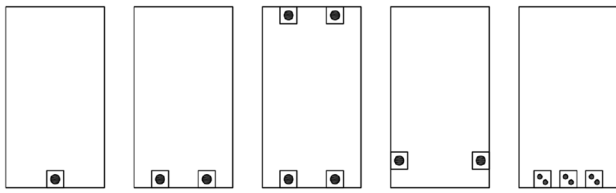


Fig. 1 Reinforcement layouts using CFRP bars

et al. (2015) and Franke et al. (2015). The first identified method of strengthening the existing structural members is the near-surface mounting of CFRP bars with epoxy glue (Fig. 1). Such studies were carried out, among others, by Raftery and Whelan (2014) and Bergner et al. (2018). Bars can be pre-stressed as well, which was proposed by Yang et al. (2016a).

The second way is to reinforce wood with CFRP mats, tapes or strips. This can be done on a variant width of the cross-section, as L or U profiles (Fig. 2). Such reinforcements were analysed, among others, by Andor et al. (2015), de la Rosa Garcia et al. (2016), Rescalvo et al. (2017), Nadir et al. (2016), Vahedian et al. (2019), Brunetti et al. (2019), Subhani et al. (2017), and Zhang et al. (2022). CFRP tapes can be pre-stressed as well, which was investigated by Halicka and Ślósarz (2021, 2022).

The last method of strengthening the girders is cutting the cross-section and gluing the CFRP strips into the prepared incisions (Fig. 3). This approach was checked by Jankowski et al. (2010), Nowak et al. (2013) and Morales-Conde et al. (2015).

Another group of reinforced wooden elements are beams made by joining wood with CFRP at the stage of their production, by gluing CFRP tapes between wooden lamellas, in various arrangements (Fig. 4). The necessity to apply an adequate pressure of the composite components to get a strong adhesive layer determines using CFRP tapes or strips only. Such studies were carried out, among others, by Raftery and Harte (2011) and Raftery and Rodd (2015), Glišović et al. (2016), Yang et al. (2016b), He et al. (2022), and the author of this paper (Kawecki and Podgórski 2020b; Kawecki 2021a).

In summary, the presented configurations of strengthening or reinforcing wood are very diverse. On the other hand, a thorough review of the literature showed not a large amount of information on the fire resistance of such composites. This proves the significant importance of the topic presented in this paper.

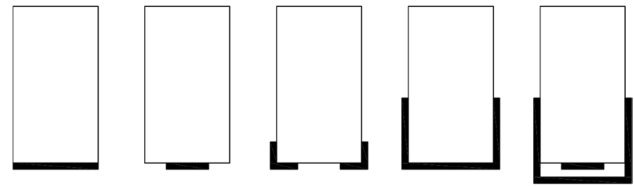


Fig. 2 Reinforcement layouts using CFRP mats, tapes or strips

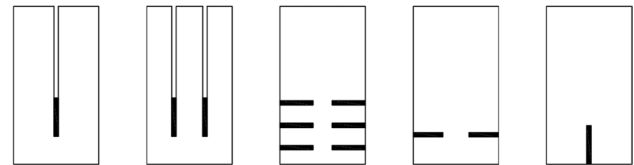


Fig. 3 Reinforcement layouts using CFRP strips glued in incisions

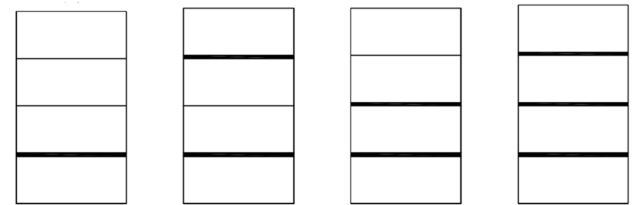


Fig. 4 Layouts of wood-CFRP composites combined at the stage of their production

1.2 Combustion tests on glue laminated timber and wood-CFRP composites

Despite the technological progress, structural-sized fire tests are still a big challenge for researchers. Only a few research centres worldwide are dealing with wooden products combustion under static loading. The evidence is a low number of scientific publications in this field. Conducting the research on loaded structural-sized samples in a laboratory is problematic and generates very high costs. The reason is a necessity to protect expensive laboratory equipment, such as testing machines, force actuators, displacement sensors, etc., from destruction by high temperature and fire. In order to limit the range of fire exposure, researchers try to burn specimens only in the most loaded cross-section (region of highest bending moment). It enables to reduce the size of the fire source several times and to keep a sense of the mechanical behaviour of the member in fire.

The first group of tests includes applying the load before starting a fire exposure and remaining it constant during experiments. Such tests on fast growing tropical wood were performed by Firmanti et al. (2004, 2006) starting with

small-scale specimens with dimensions of $20 \times 20 \times 500$ mm (Firmanti et al. 2004) and continuing with structural-sized beams with dimensions of $60 \times 120 \times 3500$ mm (Firmanti et al. 2006). They focused on the relationship between stress level and fire resistance in a four-point bending test with heated zone set in the middle of the beam at one-third of its span. Similar tests were performed by Qin et al. (2021). They tested small-scale specimens with dimensions of $50 \times 50 \times 500$ mm made of three different wood species in four-point bending and the heated zone equal to 50 mm. They stated that the stress level has a significant influence on the failure time.

The behaviour of glued timber was investigated by Schmid et al. (2010) who considered two types of cross laminated timber (CLT) panels with dimensions of $150 \times 95 \times 3300$ mm and $150 \times 150 \times 2700$ mm in four-point bending with heated zone equal to 1 m. They prepared eight samples, four of them were heated in tension zone and four in compression zone. Lineham et al. (2016) studied the structural response of twelve 2 m long (1.9 m span between supports) and 100 mm high CLT beams under four-point bending in two layouts, five-layer and three-layer beams. The heating zone was equal to 300 mm. Chen et al. (2017) tested one structural-sized simply supported glue laminated timber (BSH) beam with dimensions of $300 \times 480 \times 4700$ mm loaded with uniformly distributed load equal to 0.8 kN/m. In this test, the entire beam was placed in the furnace. Fahrni et al. (2019) conducted a four-point bending test on six samples of BSH beams with dimensions of $160 \times 250 \times 3800$ mm. The beams were loaded at a level of 30% of their real load bearing capacity. The heated zone was 1.5 m wide and was set in the middle of the beam. Wang et al. (2020) tested six samples of CLT panels with dimensions of $420 \times 105 \times 2200$ mm. They applied three levels of load, at: 8%, 14% and 18% of the bearing capacity of panels.

The second group of tests includes exposure of samples to fire before load application, so-called post-fire behaviour. This approach does not consider a real-time fire exposure of loaded elements, and in consequence may not show the real behaviour of the structural elements in fire. Such tests on BSH beams with dimensions of $140 \times 270 \times 1800$ mm and $190 \times 270 \times 1800$ mm made of five different wood species were performed by Yang et al. (2009). The samples were placed in the furnace for various fire exposure times, then cooled down to room temperature and finally subjected to a three-point bending. The heating zone was 900 mm, and was set in the middle of the beam. Quiquero et al. (2018) studied five BSH beams with dimensions of $45 \times 195 \times 4200$ mm after short-term fire exposure. They burned the samples on the length of 1 m to reach charring depth of 5 mm. After time of re-acclimatising in the laboratory, they performed a four-point bending test. Chorlton and Gales (2020) examined

eighteen laminated veneer lumber (LVL) and ten BSH samples with dimensions of $35 \times 155 \times 800$ mm in four-point bending. The idea was to get a short-term heat exposure, leading to 5 mm and 10 mm charring depth, in two different locations—in the middle of the beam and near the bottom support.

The above mentioned papers describe experiments done on pure wood or glued timber. Recent years show no relevant interest in testing wood-FRP (fibre reinforced polymer) products under fire exposure. Last studies were conducted more than 20 years ago. Ogawa (2000) performed tests on BSH beams with dimensions of $45 \times 105 \times 1580$ mm strengthened with carbon fibre reinforced polymer (CFRP) on top and bottom side. The setup was a three-point bending test with the furnace set in the sample's centre. The load applied before ignition was at a level of two-third of the real bearing capacity. The results were optimistic—Ogawa stated that CFRP strengthening elongated the time of fracture. Martin and Tingley (2000) tested different FRP reinforcement—aramid reinforced polymer (ARP), carbon aramid reinforced polymer (CARP) and glass aramid reinforced polymer (GARP) with composite applied on the bottom side and just above the last wooden lamella. They tested beams of widths of 65 mm, 80 mm and 130 mm and different number of wooden lamellas (6, 8 or 16). The length of beams varied from 4.3 m (3.7 m—span between supports) to 6.3 m (5.5 m—span between supports). The main conclusion was that the use of FRP provided no noticeable increase in fire endurance of FRP-BSH beams comparing to pure BSH beams. Despite this, the authors stated that the placement of FRP inside the beam provided better fire performance, because wood insulated the FRP.

The papers by Ogawa (2000) and Martin and Tingley (2000) did not give enough knowledge about behaviour of wood-FRP composites. Motivation of the authors' research is to expand scientific knowledge in this field, based on recent measuring techniques, materials properties and technological regime used in producing specimens.

2 Materials and methods

2.1 Test samples

Kawecki and Podgórski (2020a, b) and Kawecki (2021a, b) confirmed assumptions of FE models used for predicting the behaviour of pure glue laminated timber and wood-CFRP composite beams (henceforth referred to as BSH and BSH-CFRP, respectively). The confirmations were based on laboratory tests of wood, adhesive layers and CFRP tapes and in terms of force–deflection relation. Determining values of stiffness (K_u) and maximal force (P_{max}) for beams with

different dimensions or changed supports required a creation of a new FE model. Figure 5 presents the fundamental assumptions for FE model according to a planned experimental setup for two selected beams.

The FE model ensured determination of the averaged values of beam stiffness and maximal force. Calculations for the beams presented in Fig. 5 resulted in the values of stiffness K_u equal to 0.803 kN/mm and 0.877 kN/mm, and in the values of maximal forces P_{max} equal to 29.45 kN and 32.35 kN, respectively for BSH and BSH-CFRP beams. Figure 6 shows the force–deflection (P/w) curves based on FE model.

In the planned experiments the behaviour of each beam should be limited to the linear-elastic one, as in real-built structures. It means no need for creating a complex, non-linear FE model for each case. For this purpose, theoretical closed-form solution may be elaborated and validated with the FE model. It also enables to use theoretical formulas for fast-calculations. To make the formulas more general, standardised BSH properties are used (PN-EN 14080 2013) in calculations. Theoretical formula for deflection of the centre of wooden beam in a three-point bending test, according to the standardised GL24h class of BSH used in the experiments is (1):

$$w = \frac{PL^3}{48E_{0,mean}J} + \frac{3PL}{10G_{mean}A} \tag{1}$$

where: P force, L span length, $E_{0,mean}$ characteristic value of a longitudinal modulus of elasticity of BSH (equal to 11.50 GPa), J bending moment of inertia, G_{mean} shear modulus (equal to 0.65 GPa), A cross-sectional area.

Simplifying the names of the samples by naming BSH samples as B and BSH-CFRP as BW and substituting J with J_B or J_{BW} and A with A_B or A_{BW} enables to calculate deflection for BSH and BSH-CFRP beams. For BSH beams (B) the formulas are (2):

$$J_B = \frac{16bh_L^3}{3}, A_B = 4bh_L, y_{0,B} = 2h_L \tag{2}$$

where: b width of a cross-section, h_L height of a single wooden lamella, $y_{0,B}$ geometric centre of a cross-section.

In case of BSH-CFRP beams (BW) the formulas are (3–7):

$$J_{BW} = J_I + J_{II} + J_{III}, A_{BW} = b(4h_L + nt_{CFRP}), n = 0.85 \frac{E_{CFRP}}{E_{0,mean}} \tag{3}$$

$$J_I = \frac{9bh_L^3}{4} + 3bh_L \left(\frac{5}{2}h_L + t_{CFRP} - y_{0,BW} \right)^2 \tag{4}$$

$$J_{II} = \frac{nb t_{CFRP}^3}{12} + nb t_{CFRP} \left(y_{0,BW} - h_L - \frac{1}{2}t_{CFRP} \right)^2 \tag{5}$$

Fig. 5 Fundamental assumptions of FE model according to the planned experimental setup

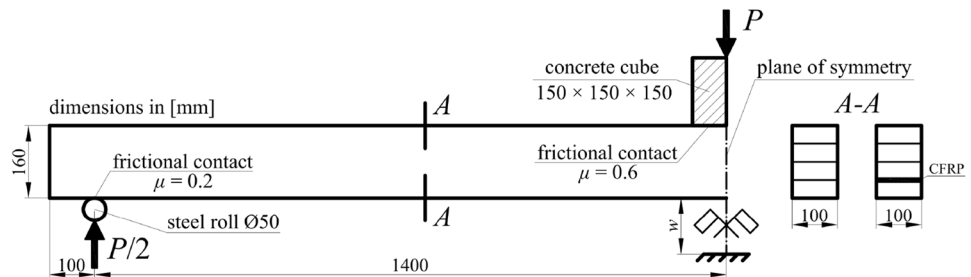
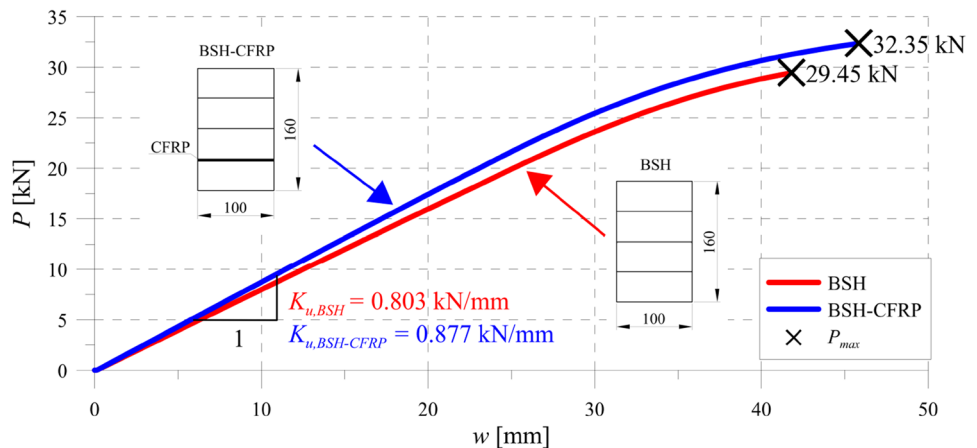


Fig. 6 Force–deflection curves from the FE model



$$J_{III} = \frac{bh_L^3}{12} + bh_L \left(y_{0,BW} - \frac{h_L}{2} \right)^2 \tag{6}$$

$$y_{0,BW} = \frac{3h_L \left(\frac{5}{2}h_L + t_{CFRP} \right) + nt_{CFRP} \left(h_L + \frac{1}{2}t_{CFRP} \right) + \frac{1}{2}h_L^2}{4h_L + nt_{CFRP}} \tag{7}$$

where: J_{BW} total bending moment of inertia of a BSH-CFRP composite, J_I component of a BSH part above CFRP tape, J_{II} component of CFRP tape, J_{III} component of the bottom BSH lamella, n reduced coefficient of elastic modules calculated from the dependency between CFRP and BSH material modulus of elasticity, t_{CFRP} thickness of CFRP tape, E_{CFRP} modulus of elasticity of CFRP tape, $y_{0,BW}$ geometric centre of a cross-section.

The formulas for an average stiffness, in comparison to the values obtained from the FE model, give 0.0% error for B beams and 0.5% error for BW beams, so the theoretical models reproduce the averaged FE stiffness very well. An expected standard deviation of the results was $\pm 11\%$, as stated in earlier experiments (Kawecki 2021a). The applied load should not exceed a load bearing capacity in a linear-elastic range—for three-point bending, the maximal forces for B and BW beams respectively, are (8):

$$P_{\max,B} = \frac{4f_m J_B}{Ly_{0,B}}, P_{\max,BW} = \frac{4f_m J_{BW}}{Ly_{0,BW}} \tag{8}$$

where: f_m characteristic value of the bending strength of BSH material.

The research presented in this paper was carried out for beams with the width of 100 mm, 120 mm and 145 mm, constant height of 160 mm and constant length of 3000 mm (span between supports equal to 2800 mm). The CFRP tapes were S&P SM C-Laminate (S&P C-Laminate Technical Card 2023) with sectional dimensions of 100×1.4 mm, 120×1.4 mm, and 150×1.2 mm and modulus of elasticity equal to 175 GPa. The widest tapes had different thickness than the others due to an unavailability of 150×1.4 mm tapes in the manufacturer's offer.

For each width two beams were made by ABIES Poland Ltd, one BSH and one BSH-CFRP. All beams consisted of four lamellas. The FRP tapes were glued over the bottom lamella in case of BSH-CFRP samples. The adhesives in each specimen (wood-wood and wood-CFRP connection)

were prepared using one-component polyurethane glue Loctite HB 110 Purbond. Figure 7 presents samples' sections used in the experiments and Fig. 8 shows preparing the elements in ABIES Poland Ltd. The discrepancy between the names of samples and the values of dimensions in the case of B_150 and BW_150 specimens resulted from the necessity of an additional grinding of lateral surfaces of the beams before the tests.

The beams were made in GL24h strength class, so its bending strength was $f_m = 24$ MPa. According to the presented theoretical model, different values of maximal force and deflection were calculated for various levels of loading (Table 1).

Loading the sample with $1.0 f_m$, $0.9 f_m$ and $0.8 f_m$ meant about 50%, 45% and 40% of load bearing capacity, respectively (compare P_{\max} for B_100 and BW_100 from Table 1 to the maximal values shown in Fig. 6). Based on Table 1, the designed experimental stand should withstand at least the load equal to 24 kN (BW_150 beam).

2.2 Experimental stand

The combustion of B and BW beams was performed on a self-designed and self-constructed experimental stand. The beams were burned in the most loaded section (region of highest bending moment) under constant loading. The idea of the stand construction was based on the lever mechanism. Single IBC 1000 L container was placed on a steel lever and was filled with the desired amount of water, that allowed controlling the loading level. Other IBC 1000 L tanks were placed on the opposite side of the lever as a counterweight. The lever was designed with HEB120



Fig. 8 Preparing the elements in ABIES Poland Ltd

Fig. 7 Cross-sections used in the experiments

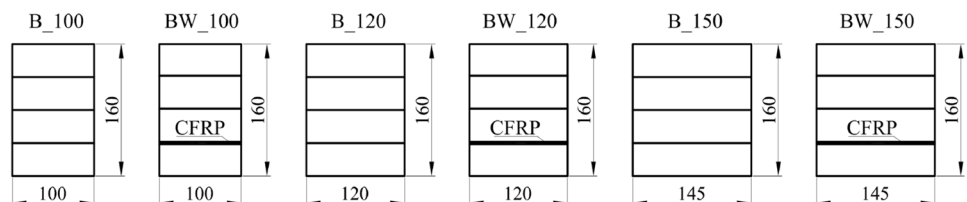


Table 1 Maximal force and deflection in dependence of loading level

Beam type	$1.0 f_m$		$0.9 f_m$		$0.8 f_m$	
	P_{max} [kN]	w_{max} [mm]	P_{max} [kN]	w_{max} [mm]	P_{max} [kN]	w_{max} [mm]
B_100	14.63	18.23	13.17	16.40	11.70	14.58
BW_100	16.69	18.93	15.02	17.04	13.35	15.14
B_120	17.55	18.23	15.80	16.40	14.04	14.58
BW_120	20.03	18.93	18.03	17.04	16.02	15.14
B_150	21.21	18.23	19.09	16.40	16.97	14.58
BW_150	23.79	18.84	21.41	16.95	19.03	15.07

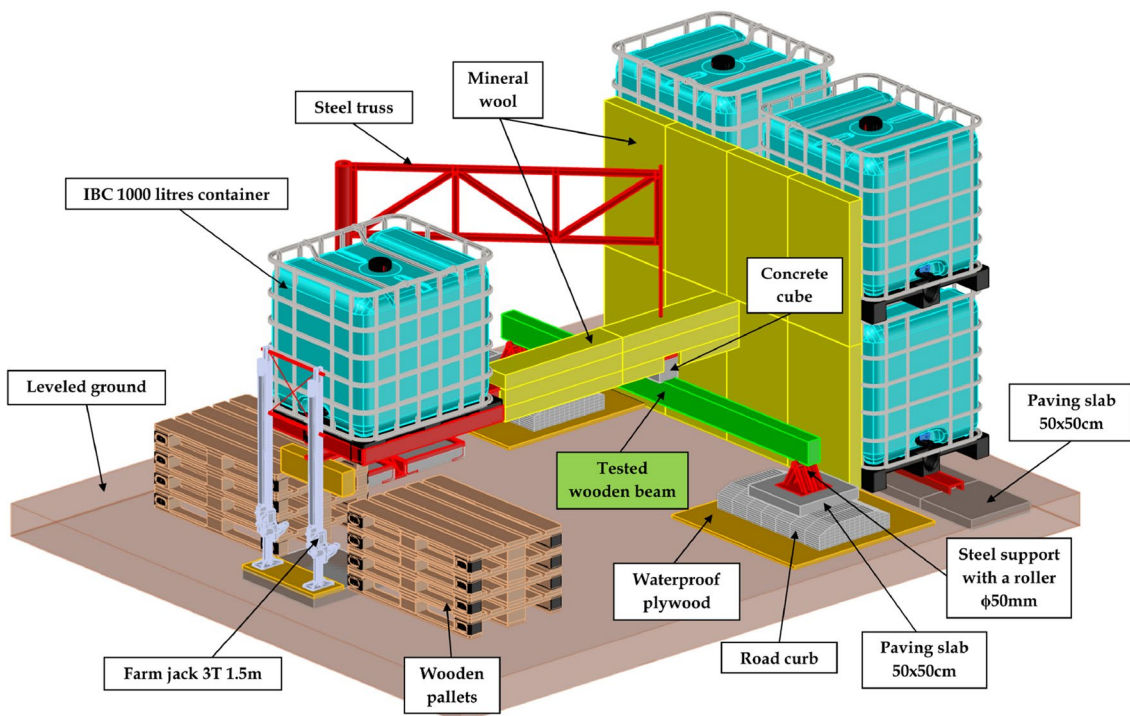
beam with the steel class S235. The bent and burned beams were arranged perpendicular to the lever and supported on two symmetrically placed supports. Combustion took place under the centre of the loaded bent beam. All components sensitive to fire and heat were insulated with mineral wool. It was planned to raise the end of the lever with a single IBC container by means of two farm jacks. A steel truss was erected next to the HEB beam, serving as a support for mounting the displacement sensor. All tests took place in the field, on the ground, that had been properly levelled and hardened prior to the installation of the stand. Figure 9 presents a conceptual visualisation of the

experimental setup, while Fig. 10 shows a static scheme of the lever mechanism.

The following notation was introduced in Fig. 10: R_B —a point load applied to the tested beam, R_A —counterweight, G_{IBC} —weight of an empty IBC container, G_W —weight of water in IBC container, G_L —weight of a steel clamp supporting the IBC container, G_C —weight of a concrete cube with steel plate and roll, g_{HEB} —weight of a steel lever. During the experiment, the value of G_W was changing according to the desired value of maximal force.

The point load applied to the tested beam (reaction of the lever in point B), R_B can be calculated from formula (9):

$$R_B = \frac{G_L(2L_1 + 2L_2 + L_3) + (G_{IBC} + G_W)\left(L_1 + L_2 + \frac{L_3}{2}\right) + G_C L_1 + g_{HEB} \frac{(L_1 + L_2 + L_3)^2}{2}}{L_1} \quad (9)$$

**Fig. 9** Visualisation of the experimental setup

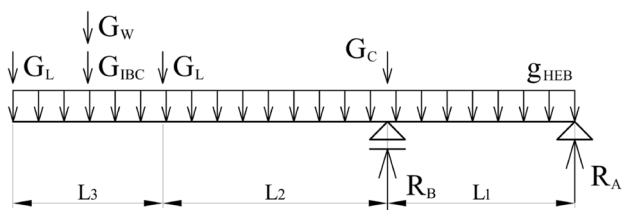


Fig. 10 Static scheme of the lever mechanism

and a needed counterweight (reaction of the lever in point A), \$R_A\$ from formula (10):

$$R_A = -R_B + G_C + 2G_L + G_{IBC} + G_W + g_{HEB}(L_1 + L_2 + L_3) \tag{10}$$

The size of stand elements considered a possibility of transport and manual assembly. Referring to this, the lengths in Fig. 10 were assumed as: \$L_1 = 1\$ m, \$L_2 = 1.8\$ m, \$L_3 = 1.2\$ m (length of the IBC container). The maximal force applied to the beams, \$R_{B,max}\$, was for the completely filled single IBC container (1000 L of water) and was equal to 38.68 kN. It was enough for tests for which the needed force for the beam with the largest section was 24 kN (compare Table 1).

2.3 Combustion time estimation

Estimation of a combustion time was based on the method described in Firmanti et al. (2004, 2006) and Fahrni et al. (2019) as well as standard (PN-EN 1995-1-2 2008). The method, illustrated in Fig. 11, involves reducing the cross-section according to charring rate (amount of wood charred in time) and zero strength layer (layer without load bearing properties).

An effective charring depth \$d_{ef}(t)\$ can be calculated from formula (11):

$$d_{ef}(t) = \beta_n t + k_0 d_0 \tag{11}$$

where: \$\beta_n\$ charring rate (for BSH equal to 0.7 mm/min), \$t\$ combustion time, \$d_0\$ depth of zero strength layer (equal

to 7 mm—standard value) and \$k_0\$ coefficient for non-protected surfaces (for simplification equal to 1.0).

The calculations were only possible for BSH beams for which the method was created. BSH-CFRP, as an innovative material, may show a different behaviour. The following formulas were used for further calculation of combustion time (12):

$$M_{max} = \frac{P_{max}L}{4}, f(t) = W(t) - \frac{M_{max}}{MOR} \tag{12}$$

where: \$P_{max}\$ force applied to the beam before combustion, \$L\$ span of the beam, \$M_{max}\$ maximum bending moment resulting from applied force, \$W(t)\$ strength index according to the fundamental theory of elasticity (dependent on time), \$MOR\$ (Modulus of Rupture) experimental bending strength of tested beams, \$f(t)\$ function representing reduction of the section in terms of experimental load bearing capacity.

The value of \$MOR\$ was based on Kawecki's (2021a) earlier work. This value strongly influences the results, because it limits an endurance of elements. It makes it necessary to assume the value of \$MOR\$ within a min–max range, which was in current analyses 34.7 ÷ 47.4 MPa. A real root of a 3rd degree polynomial expressed by Eq. (13) must be found to determine the time at which the element will collapse. The values of predicted combustion time for BSH beams and level of load established at 0.9 \$f_m\$, calculated in correspondence to \$MOR\$ limits, are presented in Table 2.

$$f(t) = \frac{1}{6} [b - 2d_{ef}(t)] \cdot [h - d_{ef}(t)]^2 - \frac{M_{max}}{MOR} \tag{13}$$

The high influence of \$MOR\$ on the combustion time (Table 2) means that any defects, such as knots or finger joints in wooden lamellas, affect its value. According to the analyses, a furnace should burn maximally for about 30 min – that was defined by the upper limit of \$MOR\$ for the largest beam taking into account the extra time.

Fig. 11 Reduced section of the beam

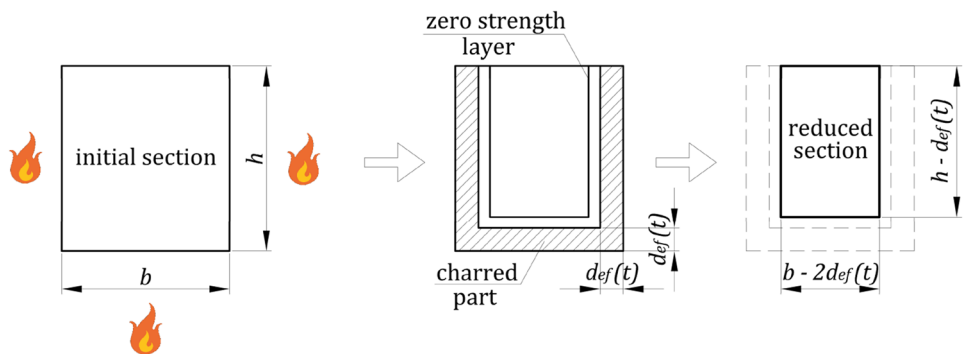


Table 2 Predicted combustion time for BSH beams at loading level equal to $0.9f_m$

MOR / Beam type	B_100	B_120	B_150
	$P_{max} = 13.17$ kN	$P_{max} = 15.80$ kN	$P_{max} = 19.09$ kN
MOR = 34.7 MPa	520 s = 8.7 min	659 s = 11.0 min	808 s = 13.5 min
MOR = 47.4 MPa	1128 s = 18.8 min	1354 s = 22.6 min	1598 s = 26.6 min

**Fig. 12** Samples for testing firewood density and moisture content

2.4 Furnace properties

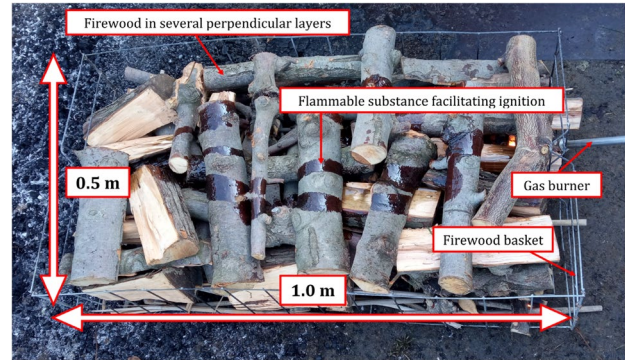
The furnace was a wood-fired basket with dimensions of $1.0 \times 0.5 \times 0.25$ m³. Firewood properties like moisture content and density were determined in the laboratory. Figure 12 shows the cylindrical samples cut from random parts of wood. Average density was equal to 690 kg/m³ and average moisture content of small slices tested in a moisture analyser was equal to 11.8%.

For such well-dried wood, its calorific value was at least 14.4 MWs/kg (Krajnc 2015; Cichy et al. 2017). The determination of a minimal amount of firewood needed in each experiment was based on the expected time of combustion and fundamental laws of physics. The provided heat energy is defined as (14):

$$Q = c_p m_p \Delta T \quad (14)$$

where: c_p specific heat of air, m_p mass of air to be heated and ΔT air heating temperature.

The typical value of specific heat for dry air is equal to 1005 J/kg °C. The estimated mass of air was calculated based on the air volume to be heated under and around the beam, $1.0 \times 0.5 \times 0.5$ m³, and air density, 1.25 kg/m³, and was equal to about 0.4 kg. Finally, the intended temperature was 800 °C. Substituting the values into Eq. (14) and accepting 30 min of burning, gives the heat energy that has to be provided as equal to 580 MWs. Assuming calorific value of wood as 14.4 MWs/kg leads to the determination of needed mass of firewood as equal to 40 kg. The entire basket completely filled with wood weighted 86 kg, so it ensured with double reserve the amount of wood for a single experiment (Fig. 13). Pieces of wood were placed in several perpendicular layers. A flammable substance and a gas burner ensured good lighting of the furnace.

**Fig. 13** The furnace description

2.5 Initial measurements before combustion

The measurement of force and displacement near the loading point preceded each combustion test. First, the initial force produced by empty IBC container was measured. It was the first validation of the correctness of the designed stand. The force value resulting from this load ($G_w = 0$) calculated with formula (9) was $R_B = 5.33$ kN, while the value of the force measured with the AXIS FB20kN force sensor was $R_B = 5.59$ kN (Fig. 14).

The measured deflection was $w = 4.39$ mm, while the calculated value, including typical standard deviation for samples, was $w = 4.22 \pm 0.46$ mm. The force error was less than 5% and deflection was within the range resulting from the calculations. It confirmed that the experimental stand worked as intended and was well-designed.

A loading level in the combustion experiment was equal to $0.9f_m$, based on Table 1. The procedure of preparation of each sample before burning test was repetitive. The first step was measurement of an initial force (P_{max}) and deflection (w_{max}) using force and LVDT sensors. In the second step sensors were replaced with a concrete cube with attached steel plate with roll providing a hinge connection during the fire test. The use of farm jacks allowed avoiding of pouring and re-pouring water between consecutive tests. Table 3 compares measured and calculated forces and deflections.

The maximal relative difference of deflections was equal to 12% like the values observed in previous experiment carried out by Kawecki and Podgórski (2020a, b) and Kawecki (2021a, b). The main reason of deviations is the unavoidable difference in the structure of the wooden elements,

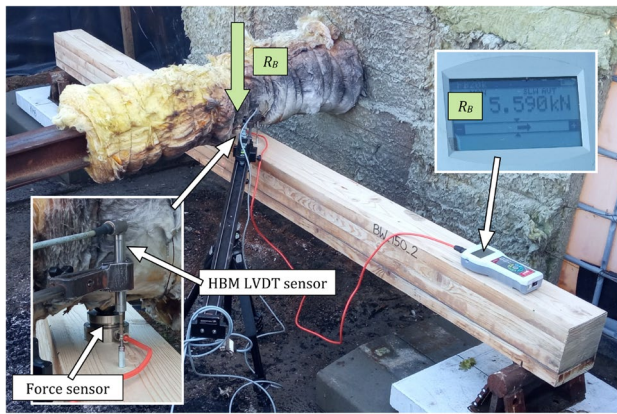


Fig. 14 Measurement of force validating the experimental stand

which cannot be taken into account at the calculation stage. However, considering the average deviations of stiffness and strength in wood members equal to 20%, the results are correct.

2.6 Temperature and deflection measurement

The temperature measuring point was in the middle of the tested beam span. A pyrometer Benetech GM1651 was used, operating in temperature range from $-30\text{ }^{\circ}\text{C}$ to $+1650\text{ }^{\circ}\text{C}$. A laser sight ensured a correct setting of the pyrometer. According to a technical card, for a distance of 1.5 m between the device and beam the measured area had a diameter equal to 42 mm. The equipment’s measurement error was 1.5% that meant $12\text{--}15\text{ }^{\circ}\text{C}$ for $800\text{--}1000\text{ }^{\circ}\text{C}$ measuring temperature. The deflection of the beam central cross-section was measured with HBM LVDT sensor mounted to the lever by a sliding rod. Simultaneously, a method based on manual processing images from two cameras (set quite far from the combusted sample, because of high temperature) was used to check the correctness of measuring displacement with LVDT sensor. The monitored part was an edge between the front and bottom planes of the concrete cube, as no-charring element

positioned in the middle of the tested beam. Details of sensors placement and assembly are presented in Fig. 15.

2.7 Weather conditions control

The stand was set outdoors. Hence, the experiment results could have been affected by the weather. The samples described in this paper were tested within 1 day to minimize the influence of external meteorological conditions. After the weather forecast was checked, a good-weather day was chosen. As another protection, the entire stand was tightly fenced with foil to decrease possible wind influences on the fire. However, low wind speed occurred during the experiment. To state that its influence was negligible, measurements with anemometer were provided. The anemometer NAVIS WL 11X/WDS was placed inside the fenced zone near the right support of the tested beams and instantaneous wind speed and direction were recorded (Fig. 16). Sampling of the equipment was 2 s and measurement accuracy 0.1 m/s. Daily relative humidity was 60% and average air temperature was $9\text{ }^{\circ}\text{C}$.

The daily averaged wind speed was equal to 0.12 m/s. The value of wind speed was enough to state that its influence may be neglected. Only several higher wind gusts occurred during the experiments, but none of them exceeded 1.3 m/s. Hourly averaged wind speed was similarly low and stable.

3 Results and discussion

Combustion tests comprised burning six beams in the middle of their span in three-point bending at load level equal to $0.9 f_m$. They included simultaneous measurements of the temperature on the surface of beam (θ) and the deflection of central cross-section (w_{fire}). The starting point for analysis of each beam was a temperature equal to $\theta = 300\text{ }^{\circ}\text{C}$, more or less corresponding to wood charring temperature.

Two criteria of member’s failure were defined according to Ryan and Robertson (1959) and PN-EN 1363-1 (2020). The first one was a rapid and visible growth of

Table 3 Measured and calculated force and deflection

Beam type	Calculated		Measured		Relative difference	
	P_{max} [kN]	w_{max} [mm]	P_{max} [kN]	w_{max} [mm]	P_{max} [%]	w_{max} [%]
B_100	13.17	16.40	13.17	16.33	0.0	0.4
BW_100	15.02	17.04	15.02	15.32	0.0	10.1
B_120	15.80	16.40	15.90	14.44	0.6	12.0
BW_120	18.03	17.04	18.10	16.70	0.4	2.0
B_150	19.09	16.40	19.03	16.48	0.3	0.5
BW_150	21.41	16.95	21.44	15.72	0.1	7.3

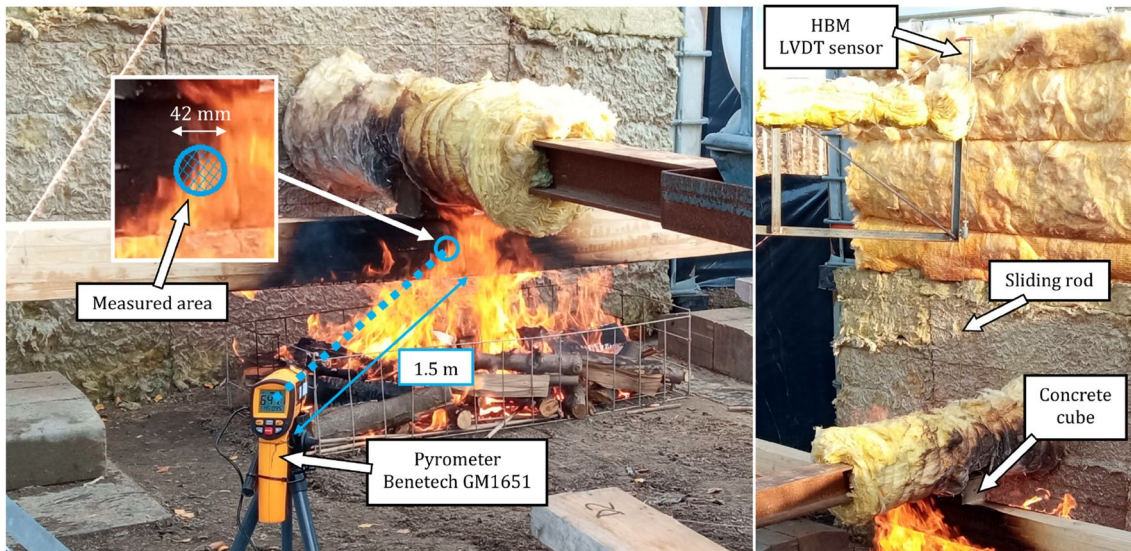
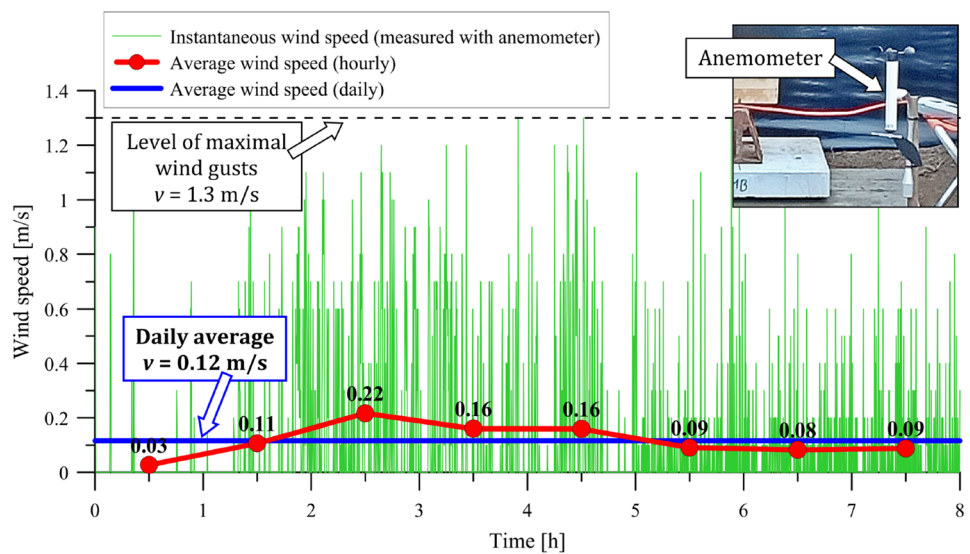


Fig. 15 Method for measuring temperature and deflection of the tested element

Fig. 16 Wind speed during the tests



displacements (R). The second one was a maximum deflection (D) used when the growth was not clearly visible (15):

$$D \geq \frac{L^2}{800h} \quad (15)$$

where: L span of the beam, h height of the beam.

Figure 17 presents temperature and deflection and Fig. 18 shows forms of combustion failure for B_100 and BW_100 beams.

The averaged temperature was similar during combustion of both beams. The stiffness in combustion was similar for

both beams that was shown by similar curves of deflection up to approximately 380 s (6.3 min). Failure criterion was a rapid growth of displacements (R). In case of BW_100 it appeared in 380 s, while for B_100 in 860 s. The deflection corresponding to these times was equal to about 20 mm and 40 mm, respectively. B_100 beam turned out to be more durable in fire than BW_100 beam. Different destruction forms occurred for each beam. It was a sudden crack of wood and collapse of the entire lever in case of B_100, while for BW_100 it was like a plastic flow of a material.

Fig. 17 Temperature and deflection for B_100 and BW_100 beams

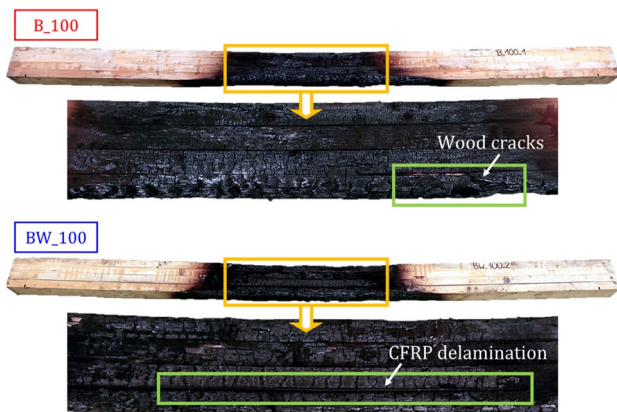
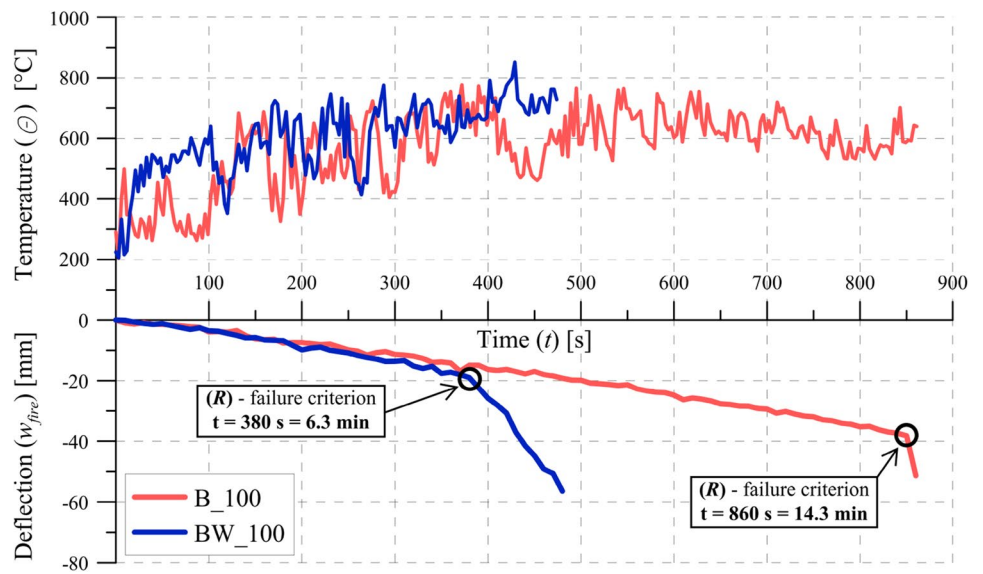
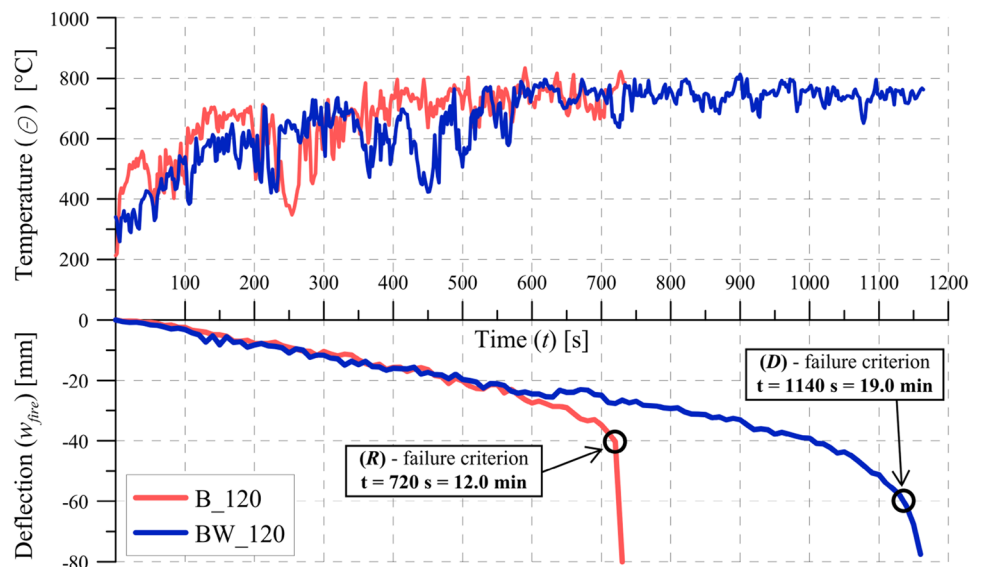


Fig. 18 Forms of combustion failure of beams B_100 and BW_100

Figure 19 presents temperature and deflection and Fig. 20 shows forms of combustion failure for B_120 and BW_120 beams.

The averaged temperature was more similar between both beams comparing to B_100 and BW_100. The stiffness in combustion was also similar for both beams up to about 600 s (10.0 min). In case of B_120 the failure criterion was a rapid growth of displacements (*R*) that appeared in 720 s (12.0 min). In case of BW_120 the displacement criterion (*D*) was used and it took place in 1140 s (19.0 min) of combustion. Deflection corresponding to the times of failure were equal to about 40 mm and 60 mm, respectively. This time BW_120 beam turned out to be more durable in fire than B_120 beam. Forms of destruction were very similar to those observed in earlier tested beams.

Fig. 19 Temperature and deflection for B_120 and BW_120 beams



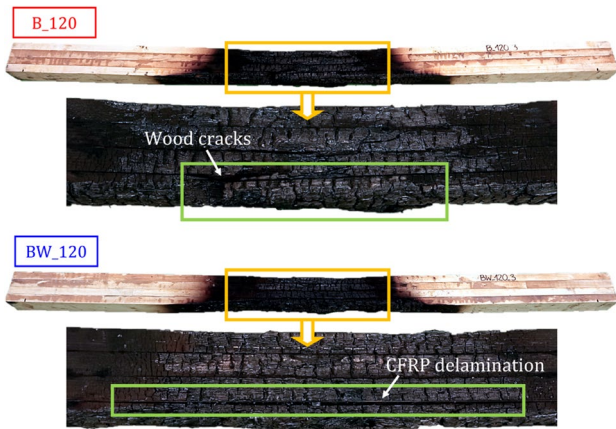


Fig. 20 Forms of combustion failure of beams B_120 and BW_120

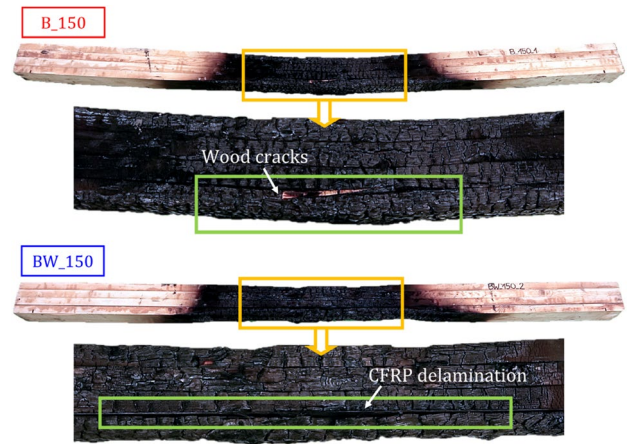


Fig. 22 Forms of combustion failure of beams B_150 and BW_150

Figure 21 presents temperature and deflection and Fig. 22 shows forms of combustion failure for B_150 and BW_150 beams.

The averaged temperature was also similar between both beams. The stiffness in combustion occurred to be different, despite similar temperature in both tests and was much lower in case of B_150. The only logical explanation was an occurrence of two finger joints in the immediate vicinity of the loading point (Fig. 23). It was the only beam with finger joints positioned in this place. This statement may be confirmed by the work of Frangi et al. (2012). The results that they obtained showed that high temperature significantly reduced both tensile and bending strength. A similar rule may be for combustion stiffness, however more detailed analysis is required in the future.

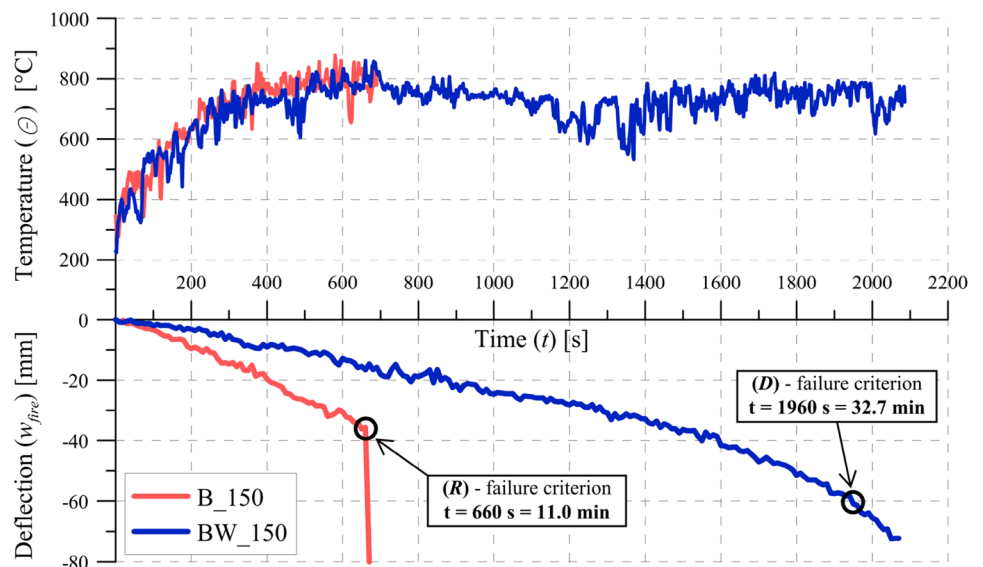
The time of rapid failure, determined as criterion (R), was 660 s (11.0 min) for B_150 and the time of reaching

criterion (D) for BW_150 was 1960s (32.7 min). The deflection corresponding to these times was about 40 mm and 60 mm, respectively. BW_150 beam turned out to be much more durable in fire than B_150 beam. Forms of destruction were very similar to those observed in remaining tests.

Worth mentioning is the discrepancy observed between prediction and measurement for the widest beam. The measured combustion time for B_100 and B_120 beams was in the range predicted in calculations, while combustion time for B_150 beam (660 s = 11.0 min) was much shorter than the lower predicted bound (808 s = 13.5 min) – compare Table 2. The finger joints, being present near the middle section, can cause this situation, as with affecting the beam’s stiffness.

Figure 24 presents results for beams of cross-sections with similar dimensions with and without CFRP tapes. It

Fig. 21 Temperature and deflection graphs for B_150 and BW_150 beams



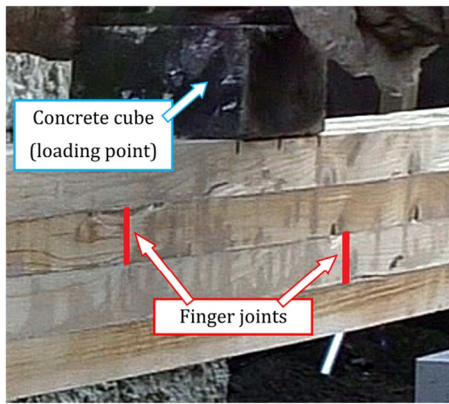


Fig. 23 Finger joints recognised in the immediate vicinity of a loading point in B_150 beam

shows an influence of CFRP tapes on the combustion time (from reaching 300 °C temperature of the element up to its fracture).

Despite the fact that a number of tested elements is not statistically valid, the trend seems to be optimistic. The results shown in Fig. 24 mean that when the width of the cross-section is increasing, a positive influence of CFRP tapes is also increasing. Probably some critical width may be determined, when CFRP tapes reduce the combustion time, which is represented by the neutral line. This conclusion can be the starting point for more detailed tests and analyses.

4 Conclusion

The paper presented tests of loaded structural-sized glue laminated timber (BSH) and innovative wooden-composite (BSH-CFRP) beams exposed to local fire burning in the

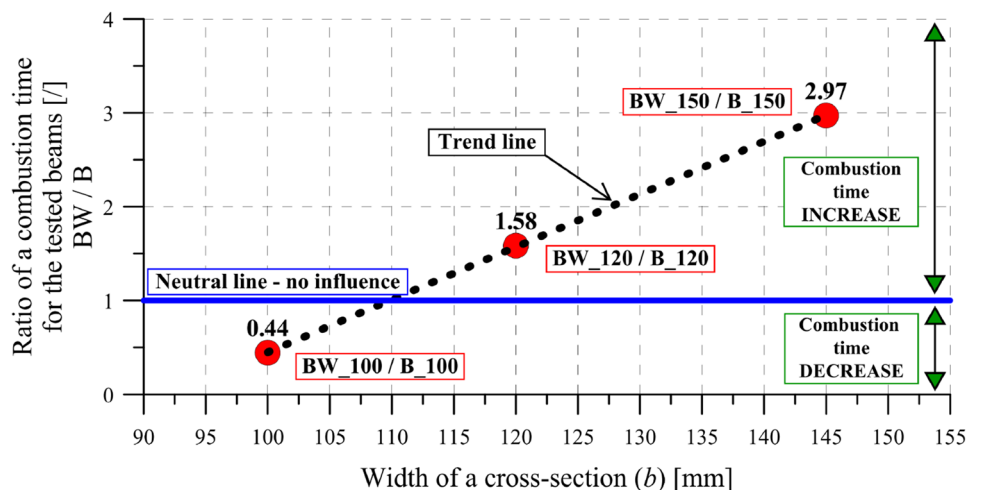
middle of their span. It showed the entire procedure from predicting the static behaviour and the combustion time of beams, designing and constructing the experimental stand, through conducting preliminary tests and discussing the results. Analyses performed in the paper may lead to several conclusions:

- FE model prepared and validated by Kawecki in his earlier works is very useful for predicting the static behaviour of BSH and BSH-CFRP beams.
- The self-designed and self-constructed experimental stand enabled applying high load and provided a stable loading during local fire exposure.
- Reduced section method used for estimating the fire-resistance of the beams gave a large scatter of results when considering the members loaded at high level, e.g. at $0.9 f_m$.
- Using CFRP tapes inside the section may both increase or decrease fire resistance of wooden members depending on the width of wood material covering CFRP tape.
- CFRP tapes provide a different nature of beam failure, which is changing from sudden fracture (BSH) to plastic flow of the material (BSH-CFRP).

Simultaneously, the authors have to state that the presented test setup and procedure are non-conventional and are not a standard method. The obtained results can be treated only as a preliminary insight into the behaviour of wood-CFRP composites in fire. Further studies, acceptable to the regulatory bodies should be conducted using a recognised international standard, such as ISO 834.

Acknowledgements We would like to thank ABIES Poland Ltd. and S&P Poland Ltd. companies for good cooperation in the field of the project.

Fig. 24 Influence of CFRP tapes on the combustion time



Author contributions Conceptualisation, B.K., M.P., T.L., A.S.; Formal analysis, B.K., M.P., T.L.; Investigation, B.K., M.P., T.L., A.S.; Methodology, B.K., M.P., T.L.; Resources, B.K., M.P., T.L., A.S.; Software, B.K.; Supervision, B.K.; Validation, B.K., M.P., T.L.; Writing—original draft, B.K.; Writing – review and editing, B.K., M.P., T.L. All authors have read and agreed to the published version of the manuscript.

Funding This research was funded by National Science Centre Poland, Grant number: 2021/05/X/ST5/00519.

Data availability The detailed data are available at link: <https://repositorium.icm.edu.pl/dataset.xhtml?persistentId=doi:10.18150/KMOJZL>.

Declarations

Conflict of interest On behalf of all authors, the corresponding author states that there is no conflict of interest.

Open Access This article is licensed under a Creative Commons Attribution 4.0 International License, which permits use, sharing, adaptation, distribution and reproduction in any medium or format, as long as you give appropriate credit to the original author(s) and the source, provide a link to the Creative Commons licence, and indicate if changes were made. The images or other third party material in this article are included in the article's Creative Commons licence, unless indicated otherwise in a credit line to the material. If material is not included in the article's Creative Commons licence and your intended use is not permitted by statutory regulation or exceeds the permitted use, you will need to obtain permission directly from the copyright holder. To view a copy of this licence, visit <http://creativecommons.org/licenses/by/4.0/>.

References

- Andor K, Lengyel A, Polgár R et al (2015) Experimental and statistical analysis of spruce timber beams reinforced with CFRP fabric. *Constr Build Mater* 99:200–207. <https://doi.org/10.1016/j.conbuildmat.2015.09.026>
- Bergner K, Tosch M, Zauer M et al (2018) Process development for the manufacture of fiber reinforced wood composites (FRWC). *Constr Build Mater* 180:275–284. <https://doi.org/10.1016/j.conbuildmat.2018.04.001>
- Brunetti M, Christovasilis IP, Micheloni M et al (2019) Production feasibility and performance of carbon fibre reinforced glulam beams manufactured with polyurethane adhesive. *Compos Part B Eng* 156:212–219. <https://doi.org/10.1016/j.compositesb.2018.08.075>
- Chen C, Yang J, Chen J et al (2017) Fire resistance performance of glulam beam. *J Cent South Univ* 24:929–936. <https://doi.org/10.1007/s11771-017-3495-8>
- Chorlton B, Gales J (2020) Mechanical performance of laminated veneer lumber and glulam beams after short-term incident heat exposure. *Constr Build Mater* 263:120129. <https://doi.org/10.1016/j.conbuildmat.2020.120129>
- Cichy W, Witczak M, Walkowiak M (2017) Fuel properties of woody biomass from pruning operations in fruit orchards. *BioResources* 12:6458–6470. <https://doi.org/10.15376/biores.12.3.6458-6470>
- de la Rosa GP, Cobo Escamilla A, González García MN (2016) Analysis of the flexural stiffness of timber beams reinforced with carbon and basalt composite materials. *Compos Part B Eng* 86:152–159. <https://doi.org/10.1016/j.compositesb.2015.10.003>
- Fahrni R, Klippel M, Just A et al (2019) Fire tests on glued-laminated timber beams with specific local material properties. *Fire Saf J* 107:161–169. <https://doi.org/10.1016/j.firesaf.2017.11.003>
- Firmanti A, Subiyanto B, Takino S, Kawai S (2004) The critical stress in various stress levels of bending member on fire exposure for mechanical graded lumber. *J Wood Sci* 50:385–390. <https://doi.org/10.1007/s10086-003-0589-8>
- Firmanti A, Subiyanto B, Kawai S (2006) Evaluation of the fire endurance of mechanically graded timber in bending. *J Wood Sci* 52:25–32. <https://doi.org/10.1007/s10086-005-0721-z>
- Frangi A, Bertocchi M, Clauß S, Niemi P (2012) Mechanical behaviour of finger joints at elevated temperatures. *Wood Sci Technol* 46:793–812. <https://doi.org/10.1007/s00226-011-0444-9>
- Franke S, Franke B, Harte AM (2015) Failure modes and reinforcement techniques for timber beams – state of the art. *Constr Build Mater* 97:2–13. <https://doi.org/10.1016/j.conbuildmat.2015.06.021>
- Glišović I, Stevanović B, Todorović M (2016) Flexural reinforcement of glulam beams with CFRP plates. *Mater Struct* 49:2841–2855. <https://doi.org/10.1617/s11527-015-0690-7>
- Halicka A, Ślósarz S (2021) Strengthening of timber beams with pre-tensioned CFRP strips. *Structures* 34:2912–2921. <https://doi.org/10.1016/j.istruc.2021.09.055>
- Halicka A, Ślósarz S (2022) Analysis of behavior and failure modes of timber beams prestressed with CFRP strips. *Compos Struct* 301:116171. <https://doi.org/10.1016/j.compstruct.2022.116171>
- He M, Wang Y, Li Z et al (2022) An experimental and analytical study on the bending performance of CFRP-reinforced glulam beams. *Front Mater* 8:1–14. <https://doi.org/10.3389/fmats.2021.802249>
- Jankowski LJ, Jasieńko J, Nowak TP (2010) Experimental assessment of CFRP reinforced wooden beams by 4-point bending tests and photoelastic coating technique. *Mater Struct* 43:141–150. <https://doi.org/10.1617/s11527-009-9476-0>
- Kawecki B (2021a) Selection of the parameters for numerical models of full girders made of wood-polymer composites reinforced with fibres. *Wydawnictwo Politechniki Lubelskiej, Lublin (in Polish)*
- Kawecki B (2021b) Guidelines for FEM modelling of wood-CFRP beams using ABAQUS. *Arch Civil Eng* 67:175–191. <https://doi.org/10.24425/ace.2021.138493>
- Kawecki B, Podgórski J (2020a) 3D ABAQUS simulation of bent softwood elements. *Arch Civ Eng* 66:323–337. <https://doi.org/10.24425/ace.2020.134400>
- Kawecki B, Podgórski J (2020b) The effect of glue cohesive stiffness on the elastic performance of bent wood-CFRP beams. *Materials (basel)* 13:1–23. <https://doi.org/10.3390/ma13225075>
- Krajnc N (2015) Wood fuels handbook. Food and Agriculture Organization of the United Nations, Pristina
- Lineham SA, Thomson D, Bartlett AI et al (2016) Structural response of fire-exposed cross-laminated timber beams under sustained loads. *Fire Saf J* 85:23–34. <https://doi.org/10.1016/j.firesaf.2016.08.002>
- Martin ZA, Tingley DA (2000) Fire resistance of FRP reinforced glulam beams. In: *Proceedings of World Conference on Timber Engineering*, July 31–August 3, Whistler Resort, Canada
- Morales-Conde MJ, Rodríguez-Liñán C, Rubio-de Hita P (2015) Bending and shear reinforcements for timber beams using GFRP plates. *Constr Build Mater* 96:461–472. <https://doi.org/10.1016/j.conbuildmat.2015.07.079>
- Nadir Y, Nagarajan P, Ameen M, Arif MM (2016) Flexural stiffness and strength enhancement of horizontally glued laminated wood beams with GFRP and CFRP composite sheets. *Constr Build Mater* 112:547–555. <https://doi.org/10.1016/j.conbuildmat.2016.02.133>
- Nowak TP, Jasieńko J, Czepizak D (2013) Experimental tests and numerical analysis of historic bent timber elements reinforced with CFRP strips. *Constr Build Mater* 40:197–206. <https://doi.org/10.1016/j.conbuildmat.2012.09.106>

- Ogawa H (2000) Architectural application of carbon fibers development of new carbon fiber reinforced glulam. *Carbon N Y* 38:211–226. [https://doi.org/10.1016/S0008-6223\(99\)00146-3](https://doi.org/10.1016/S0008-6223(99)00146-3)
- PN-EN 14080:2013 (2013) Timber structures. Glued laminated timber and glued solid timber. Requirements. Polski Komitet Normalizacyjny, Warsaw
- PN-EN 1995-1-2:2008 (2008) Eurocode 5: design of timber structures—part 1–2: general structural fire design. Polski Komitet Normalizacyjny, Warsaw
- PN-EN 1363-1:2020 (2020) Fire resistance tests—part 1: general requirements. Polski Komitet Normalizacyjny, Warsaw
- Qin R, Zhou A, Chow CL, Lau D (2021) Structural performance and charring of loaded wood under fire. *Eng Struct* 228:111491. <https://doi.org/10.1016/j.engstruct.2020.111491>
- Quiquero H, Chorlton B, Gales J (2018) Performance of adhesives in glulam after short term fire exposure. *Int J High-Rise Build* 7:299–311. <https://doi.org/10.21022/IJHRB.2018.7.4.299>
- Raftery GM, Harte AM (2011) Low-grade glued laminated timber reinforced with FRP plate. *Compos Part B Eng* 42:724–735. <https://doi.org/10.1016/j.compositesb.2011.01.029>
- Raftery GM, Rodd PD (2015) FRP reinforcement of low-grade glulam timber bonded with wood adhesive. *Constr Build Mater* 91:116–125. <https://doi.org/10.1016/j.conbuildmat.2015.05.026>
- Raftery GM, Whelan C (2014) Low-grade glued laminated timber beams reinforced using improved arrangements of bonded-in GFRP rods. *Constr Build Mater* 52:209–220. <https://doi.org/10.1016/j.conbuildmat.2013.11.044>
- Rescalvo F, Valverde-Palacios I, Suarez E, Gallego A (2017) Experimental comparison of different carbon fiber composites in reinforcement layouts for wooden beams of historical buildings. *Materials (Basel)* 10:1113. <https://doi.org/10.3390/ma10101113>
- Ryan JV, Robertson AF (1959) Proposed criteria for defining load failure of beams, floors, and roof constructions during fire tests. *J Res Natl Bur Stand Sect C Eng Instrum* 63C:121–124
- S&P C-LAMINATE Technical Information (2023). https://www.sp-reinforcement.pl/sites/default/files/field_product_col_doc_file/c-laminates_polska_ver012019-low.pdf
- Schmid J, König J, Köhler J (2010) Fire-exposed cross-laminated timber - Modelling and tests. *World Conf Timber Eng* 4:3268–3276
- Schober K-U, Harte AM, Kliger R et al (2015) FRP reinforcement of timber structures. *Constr Build Mater* 97:106–118. <https://doi.org/10.1016/j.conbuildmat.2015.06.020>
- Subhani M, Globa A, Al-Ameri R, Moloney J (2017) Flexural strengthening of LVL beam using CFRP. *Constr Build Mater* 150:480–489. <https://doi.org/10.1016/j.conbuildmat.2017.06.027>
- Vahedian A, Shrestha R, Crews K (2019) Experimental and analytical investigation on CFRP strengthened glulam laminated timber beams: full-scale experiments. *Compos Part B* 164:377–389. <https://doi.org/10.1016/j.compositesb.2018.12.007>
- Wang Y, Zhang J, Mei F et al (2020) Experimental and numerical analysis on fire behaviour of loaded cross-laminated timber panels. *Adv Struct Eng* 23:22–36. <https://doi.org/10.1177/1369433219864459>
- Yang TH, Wang SY, Tsai MJ et al (2009) Effect of fire exposure on the mechanical properties of glued laminated timber. *Mater Des* 30:698–703. <https://doi.org/10.1016/j.matdes.2008.05.022>
- Yang H, Ju D, Liu W, Lu W (2016a) Prestressed glulam beams reinforced with CFRP bars. *Constr Build Mater* 109:73–83. <https://doi.org/10.1016/j.conbuildmat.2016.02.008>
- Yang H, Liu W, Lu W et al (2016b) Flexural behavior of FRP and steel reinforced glulam beams: Experimental and theoretical evaluation. *Constr Build Mater* 106:550–563. <https://doi.org/10.1016/j.conbuildmat.2015.12.135>
- Zhang C, Chun Q, Wang H et al (2022) Experimental study on the flexural behaviour of timber beams strengthened with high ductility and low cost hybrid fibre sheets. *Constr Build Mater* 322:126514. <https://doi.org/10.1016/j.conbuildmat.2022.126514>

Publisher's Note Springer Nature remains neutral with regard to jurisdictional claims in published maps and institutional affiliations.